

U-Verse: A Miniaturized Platform for End-to-End Closed-Loop Implantable Internet of Medical Things Systems

Raffaele Guida
Northeastern University
Boston, MA, USA
guidar@ece.northeastern.edu

Neil Dave
Northeastern University
Boston, MA, USA
dave.ne@husky.neu.edu

Francesco Restuccia
Northeastern University
Boston, MA, USA
frestuc@northeastern.edu

Emre Can Demirors
Northeastern University
Boston, MA, USA
edemirors@ece.northeastern.edu

Tommaso Melodia
Northeastern University
Boston, MA, USA
melodia@northeastern.edu

ABSTRACT

The promise of real-time detection and response to life-crippling diseases brought by the Implantable Internet of Medical Things (IIoMT) has recently spurred substantial advances in implantable technologies. Yet, existing devices do not provide at once the miniaturized end-to-end sensing-computation-communication-recharging capabilities to implement IIoMT applications. This paper fills the existing research gap by presenting U-Verse, the first FDA-compliant rechargeable IIoMT platform packing sensing, computation, communication, and recharging circuits into a penny-scale platform. U-Verse uses a single miniaturized transducer for data exchange and for wireless charging. To predict U-Verse's performance, we (i) derive and experimentally validate a mathematical model of U-Verse's charging efficiency; and (ii) experimentally calculate the resistance-reactance parameters of our ultrasonic transducer and rectifying circuit. We design a matching circuit to maximize the amount of power transferred from the outside. We also go through the challenge of fabricating a full-fledged cm-scale printed circuit board (PCB) for U-Verse. Extensive experimental evaluation indicates that U-Verse (i) is able to recharge a 330mF and 15F energy storage unit – several orders of magnitude higher than existing work – respectively under 20 and 60 minutes at a depth of 5cm; (ii) achieves stored charge duration of up to 610 and 40 hours in case of battery and supercapacitor energy storage, respectively. Finally, U-Verse is demonstrated through (i) a closed-loop application where a periodic sensing/actuation task sends data via ultrasounds through real porcine meat; and (ii) a real-time reconfigurable pacemaker.

CCS CONCEPTS

• **Hardware** → *PCB design and layout*; • **Networks** → *Network measurement*; • **Human-centered computing** → *Ubiquitous and mobile devices*.

Permission to make digital or hard copies of all or part of this work for personal or classroom use is granted without fee provided that copies are not made or distributed for profit or commercial advantage and that copies bear this notice and the full citation on the first page. Copyrights for components of this work owned by others than ACM must be honored. Abstracting with credit is permitted. To copy otherwise, or republish, to post on servers or to redistribute to lists, requires prior specific permission and/or a fee. Request permissions from permissions@acm.org.

SenSys '19, November 10–13, 2019, New York, NY, USA

© 2019 Association for Computing Machinery.

ACM ISBN 978-1-4503-6950-3/19/11...\$15.00

<https://doi.org/10.1145/3356250.3360026>

KEYWORDS

Platform, Ultrasound, Charging, Wireless, IoT, Medical

ACM Reference Format:

Raffaele Guida, Neil Dave, Francesco Restuccia, Emre Can Demirors, and Tommaso Melodia. 2019. U-Verse: A Miniaturized Platform for End-to-End Closed-Loop Implantable Internet of Medical Things Systems. In *SenSys '19: Conference on Embedded Networked Sensor Systems, November 10–13, 2019, New York, NY, USA*. ACM, New York, NY, USA, 13 pages. <https://doi.org/10.1145/3356250.3360026>

1 INTRODUCTION

Connecting medical devices and personnel to networks – and to patients – is rapidly becoming big business. Experts forecast the *Internet of Medical Things* (IoMT) market will exceed \$534.3B by 2025, expanding at a CAGR of 20.2% per year [15].

From a medical perspective, the opportunities that implantable IoMT (IIoMT) platforms will offer to both doctors and patients are unprecedented in healthcare history. Through the implantation of tiny networked devices inside our bodies, healthcare professionals will be able to perform 24/7 *in situ* monitoring of critical physiological conditions without being in proximity of the patient [35]. This promise comes at a moment when healthcare expenditures in the United States have reached over \$3T a year [13], urging widespread marketization of platforms that can not only detect, but also react in real time to abnormal medical conditions. The IIoMT is expected to radically transform the healthcare landscape by allowing (i) early diagnosis and prevention of diseases through remote patient monitoring [6]; (ii) faster delivery of healthcare services and response to sudden life-threatening events [27]; (iii) reducing health care expenditure drastically [1].

Motivation. Millions of people would benefit from IIoMT systems where blood pressure and glucose sensors detect arrhythmia, hypertension and diabetes [25, 33] and implantable pumps deliver hypertension and insulin medication only when most needed [48, 49] – for example, through remote real-time intervention by healthcare professionals. Our vision, simply put, is to realize *end-to-end* implantable systems able to finally bridge the existing gap between doctors and real-time sensing/actuation of health-critical functions. The harsh reality, indeed, is that the above (and similar) IIoMT systems do not yet exist, and this is not without a reason. Despite the numerous recent advances in intra-body communications

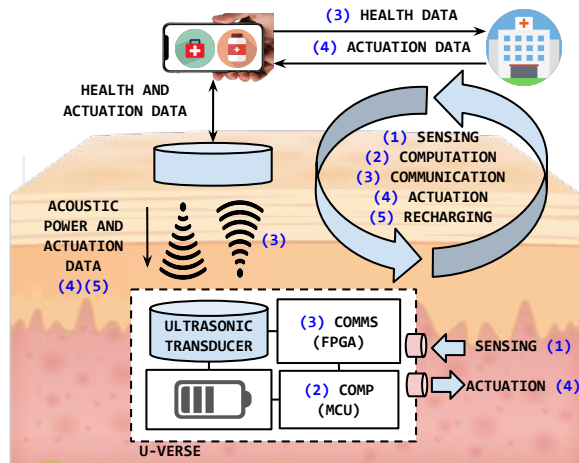


Figure 1: U-Verse enables end-to-end closed-loop long-lasting Internet of Implantable Medical Things applications.

and implantable medical devices (IMDs) – discussed in details in Section 7) – most of existing IMDs focus on small-scale ad hoc design, wireless charging, passive communications and extremely low power consumption [7–10, 46, 47], while other platforms [37, 38] focus on the computation/communication side but come short on size and miniaturization. In other words, we still lack end-to-end IIoMT systems where sensing, computation, communication and actuation work smoothly together to implement *end-to-end, real-time, long-lasting, closed-loop, miniaturized IIoMT platforms*.

Scope. This paper addresses the current research gap with the U-Verse platform. Figure 1 depicts an overview of the main components of U-Verse, while Figure 2 shows a miniaturized, penny-scale prototype. In a nutshell, U-Verse implements a platform where (i) a single ultrasonic transducer is used for data transfer and wireless charging; (ii) a miniaturized field-programmable gate-array (FPGA) and micro-controller (MCU) provide the necessary computation/communication needs. U-Verse has been specifically designed to enable highly-demanding next-generation IIoMT functionalities such as muscle/nerve stimulation, pacemaking, distributed intra-body sensing and multi-point actuation, among others.

The overarching target of this paper is to provide a blueprint for next-generation IIoMT platforms. For this reason, we focus on the design and implementation of U-Verse’s most fundamental building blocks and functionalities (*i.e.*, charging, communication, processing), which we anticipate to be key components of next-generation IIoMT applications. To demonstrate the applicability of U-Verse to a wide variety of IIoMT scenarios, in Section 6 we (i) investigate and report the discharge time for three different IIoMT closed-loop tasks; and (ii) we report preliminary results on the discharge time of a reconfigurable pacemaker implemented on U-Verse, where the pacing is established through an output pin.

Novelty. The novelty of U-Verse with respect to existing implantable devices is that it provides the first demonstration of a multi-purpose integrated and modular implantable ultrasonic IIoMT platform with sensing/communication/computation/energy harvesting. These unique capabilities enable U-Verse to achieve the following key IIoMT objectives: (i) periodically transmit outside

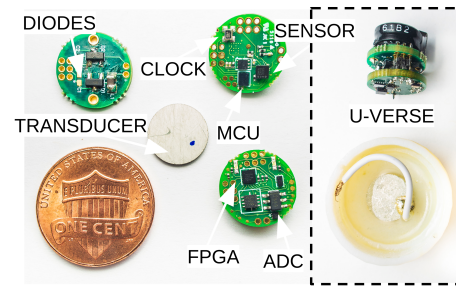


Figure 2: From top-left, clockwise: energy harvesting unit (EHU), processing and communication unit (PCU) top and bottom side, penny, and ultrasonic transducer. The dashed box shows the full stack-up with a supercapacitor as power storage, as well as the transducer location.

the body critical health-related statistics measured by implantable sensors; and (ii) control appropriate actuation to health-critical events – establishing the opportunity to implement pacing devices, smart drug pumps, and other IIoMT medical devices. To the best of our knowledge, no other IIoMT platform provides at once wireless charging, connectivity, and reconfigurability both at the communication and computation levels. From a technical perspective, one of the core innovations brought by U-Verse is that energy harvesting and ultrasound communication rely on a *single* ultrasonic interface. This aspect of U-Verse is not only novel, but also crucial as it allows to decrease the platform’s space – which significantly aids miniaturization as well as decreasing overall energy consumption and manufacturing costs.

Design Constraints and Challenges. Instead of using electromagnetic (EM) waves, U-Verse leverages ultrasound-based recharging and communication. This is because ultrasound waves have significantly lower absorption in human tissues, *e.g.*, around 70 dB less attenuation for a 1 MHz ultrasonic link vs a 2.45 GHz RF link [14, 23, 40], making them significantly more reliable than RF waves.

On the other hand, achieving miniaturized ultrasonic wireless recharging and communications is extremely challenging from a technical standpoint. First, to use a single transducer and thus avoid increasing the platform size, we had to (i) leverage a photodiode-based miniaturized relay that activates the power/communication line depending on the power received on the transducer line; (ii) design and implement a rectifying circuit to transform the AC current received by the transducer to a DC current able to recharge the energy storage; (iii) leverage a low-dropout regulator to limit the voltage delivered to the processing and communication unit. Part of our efforts included utilizing strictly commercial off-the-shelf (COTS) components and materials for both our evaluation board and our printed board circuit (PCB) prototype.

Another key challenge was deriving a mathematical model of the amount of energy that was transferable through the ultrasonic transducer given the implant’s depth and an input electrical power at the transmitter’s side. This step was necessary for two reasons. First, the United States Food and Drug Administration (FDA) imposes strict limitations in the usage of waves in human tissues – respectively, 720 mW/cm² and 10 mW/cm² for ultrasound and EM radiation [12]. Thus, although ultrasonic waves can be transmitted

with $\sim 70\times$ more power than EM waves, we still need to determine which FDA-compliant ultrasonic frequency and power are optimal to achieve relatively short recharging time. This requires a fundamental understanding of the electro-acoustic properties of the ultrasound transducer – which is traditionally used for communications only – to determine (i) its electrical-to-acoustic conversion efficiency and (ii) its resistance-reactance parameters, so as to maximize the amount of power transferred from the outside, according to Jacobi’s law [43]. Second, it is fundamental to provide the patient with accurate recharging time of the platform, so as to provide continuous monitoring of vital functions without interruptions.

Last but not least, another concern of ours was the platform’s *versatility* – indeed, an IIoMT platform should be amenable to be *reconfigured* on both the computation and communication sides. For this reason, we struggled to find the “sweet spot” between flexibility and efficiency. We addressed this issue by relying on a mm-size micro-controller (MCU) and field-programmable gate array (FPGA) design. Specifically, the MCU provides general-purpose computation while the FPGA implements a wideband ultrasonic physical-layer communication system [39] that can be reconfigured from the MCU through serial peripheral interface (SPI) registers.

Novel Contributions

This paper makes the following novel contributions:

- We propose U-Verse, the first end-to-end implantable platform closing the loop between sensing, computation, communication, actuation and recharging in the IIoMT;
- We derive and validate through experiments a mathematical model of the charging efficiency of U-Verse, and prove through experimental evaluation that the recharging process is compliant with FDA regulations;
- We design and fabricate an evaluation board and a miniaturized printed circuit boards (PCB) for U-Verse;
- We evaluate through extensive experiments U-Verse. Our results indicate that U-Verse (i) is able to recharge a 330 mF and 15 F energy storage unit, which is several orders of magnitude higher than existing work, respectively under 20 and 60 minutes at a depth of 5 cm; (ii) achieves charge duration of up to 610 and 40 hours in case of battery and supercapacitor energy storage, respectively.
- The end-to-end charging, communication, and actuation capabilities of U-Verse are further demonstrated through (i) a closed-loop application where a periodic sensing-actuation task sends data via ultrasounds through two types of porcine meat; and (ii) a reconfigurable pacemaker.

2 U-VERSE: SYSTEM OVERVIEW

Figure 3 depicts a high-level overview of the main blocks of U-Verse and the interactions among them. U-Verse realizes the vision of a self-contained IIoMT platform where sensing, computation, wireless communication and charging coexist with each other yet kept logically and physically separated for modularity purposes.

Perhaps the most fundamental design feature of U-Verse is its capability to go beyond the highly-specialized designs and architectures crippling most of existing implantable devices – and provide a “blueprint” for future IIoMT-ready devices that use ultrasound

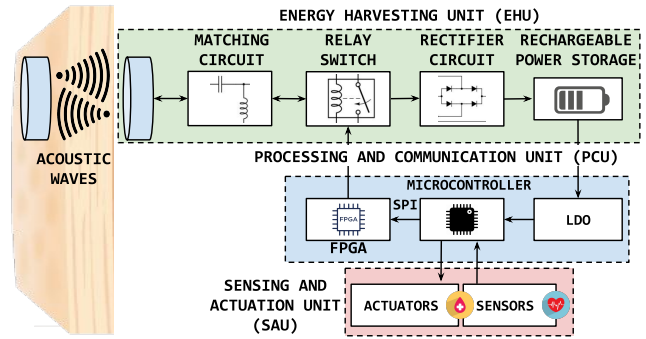


Figure 3: U-Verse is logically divided into an energy harvesting unit (EHU), a processing and communication unit (PCU) and a sensing and actuation unit (SAU).

technologies to communicate wirelessly through body tissues. Although we use specific hardware components in our prototype and printed circuit board (PCB), the key components of U-Verse (supercapacitors, transducers, sensors, etc) are entirely available off the shelf. This required to consider modularity and extendability as top priority in designing U-Verse, which obviously trades size and power consumption off to achieve the high levels of flexibility required by the IIoMT environment. Part of this design principle clearly justifies our choice to include a micro controller unit (MCU) and a mm-size field-programmable gate array (FPGA) as core components of U-Verse.

Main Modules and Operations

U-Verse is composed by (i) an energy harvesting unit (EHU), tasked with powering the computational and sensing components of U-Verse; (ii) a processing and communication (PCU) unit, which handles networking and computation tasks; and (iii) a sensing and actuation unit (SAU), which includes the circuitry necessary to implement applications such as telemetry and remote delivery of health-care services.

Energy Harvesting Unit (EHU). To recharge the platform, an alternating current (AC) square wave (or sinusoidal) signal is generated at ultrasonic frequencies (*i.e.*, > 20 kHz) from an external charger. The signal drives a piezoelectric transducer that converts the electric signal to ultrasounds. Acoustic waves are essentially mechanical waves, and as such, they need a medium to propagate. In this case the medium is represented by the human tissues. To actually transfer energy to the receiver, a piezoelectric transducer, included in the EHU, transforms the mechanical excitation back into an electrical AC signal. We presented a non optimized version of a transcutaneous energy transfer system in [19]. To improve the overall performance, we include (i) a matching circuit to transfer the maximum amount of power from the outside (Section 3.4); and (ii) a photodiode-based relay to switch the transducer from/to charging to/from communication (Section 3.5). Since the U-Verse rechargeable energy storage (*i.e.*, both supercapacitor and battery) requires a direct current (DC) voltage to recharge, we include a rectifier to generate a DC voltage from an oscillating AC input (Section 3.3). To protect the circuitry, we also include a low dropout (LDO) regulator to limit the voltage delivered to the PCU.

Processing and Communication Unit (PCU). The PCU is composed by an MCU and an FPGA, which together offer the required low-power small-area hardware and software computation and communication capabilities. The MCU is general-purpose in nature and is in charge of data processing and of executing software-defined functionalities such as sensing and applications. Conversely, the FPGA is tasked with implementing an ultrasonic wide-band (USWB) physical-layer communication scheme [39], which will be discussed in details in Section 4.2.

The usage of an FPGA instead of an application-specific integrated circuit (ASIC) guarantees physical-layer reconfigurability, which is critical for the following reasons. First, the IIoMT is still in its infancy – therefore, major wireless-related advances are expected to happen between now and a few years. Therefore, we need to be able to radically change the physical-layer fabric of the IIoMT platform to keep the pace of innovation. Second, similar to underwater systems, intrabody channels are extremely hard to model [28, 36, 39], which may require the real-time modification of physical-layer parameters (e.g., transmission gain, modulation scheme, coding levels, and so on).

Sensing and Actuation Unit (SAU). Beyond providing general-purpose computational power, the core idea behind the MCU is to interface U-Verse with a wide variety of sensors and actuators through standardized analog and digital interfaces (e.g., SPI, UART, I2C, etc). This crucial aspect indeed realizes a "plug-n-sense" vision where IIoMT platforms are flexible enough to connect with different sensors depending on the application and therapy requirements. The role of the "plug-n-sense" interface is to seamlessly connect different types of sensors to the platform without the need of re-designing the board for each sensor. Although in our current prototype a sensor is integrated in the PCB containing the PCU to decrease space, it is not challenging to realize a separate PCB containing different sensors and actuators.

3 ENERGY HARVESTING UNIT (EHU)

We first derive a mathematical model of the EHU energy transfer efficiency in U-Verse in Section 3.1. Then, we investigate the characteristics of the ultrasonic transducer in Section 3.2, followed by a characterization of the rectifier circuits in Section 3.3, a discussion on the matching network used for to maximize the amount of transferred power in Section 3.4, and a description of the solid state relay in Section 3.5. Finally, we verify that U-Verse respects FDA power limits in Section 3.6

3.1 Power Transfer Model

Why do we need a power transfer model? Deriving a predictive model of the EHU's recharging efficiency is fundamental to obtain the recharging time of the U-Verse's energy storage as a function of the platform location inside the body. Although it is intuitive that due to the increased acoustic power loss between the transducers a deeper IIoMT platform will require more charging time (or equivalently, more transmission power), it is paramount to provide accurate recharging times to the patient so that U-Verse can operate continuously.

At this point, one might say: why don't we just significantly increase the transmitter's power to solve the issue? Unfortunately, we cannot do that because in the United States, the FDA sets the

exposure limits of the human body to 720 mW/cm^2 for acoustic waves and to 10 mW/cm^2 for EM waves. This considerable difference is due to the fact that ultrasonic waves propagate better in aqueous media, resulting in a smaller absorption ratio when compared to RF [17, 38]. However, the FDA safety limitations that apply to ultrasonic waves still translate into strict design constraints that must be met, which implies that an analytical model is necessary to understand if and how the constraint on charging time can also be met by the FDA limits on maximum power transmission.

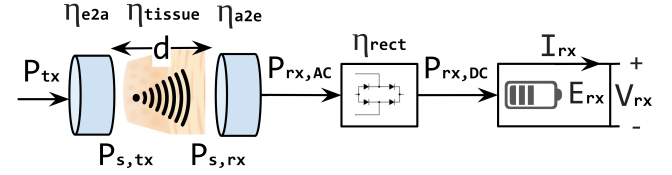


Figure 4: Power transfer model.

Figure 4 shows our mathematical model for the power transfer efficiency of the EHU. Specifically, the received power P_{rx} at the storage's side can be expressed as a function of the output of the external power generator (charger) P_{tx} as:

$$P_{rx} = P_{tx} \cdot \eta_{e2a} \cdot \eta_{tissue} \cdot \eta_{a2e} \cdot \eta_{rect}. \quad (1)$$

Let us examine each component on the right side of Equation 1. First, the quantity P_{tx} is known since it is the power used at the transmitter side. Next, η_{e2a} and η_{a2e} account for the transducer electrical-to-acoustic and the acoustic-to-electrical conversion efficiency values (considered as equal for simplicity), which we derive in Section 3.2. We derive η_{tissue} by assuming that the attenuation in soft tissues is 1 dB/cm/MHz [3, 18]. Thus, for example, the attenuation of a 700 kHz ultrasonic wave in 10 cm of soft tissue is equal to 7 dB . Finally, η_{rect} is the rectifier efficiency, which is computed in Section 3.3. We will use Equation (1) to calculate the charging time in Section 6.1.

3.2 Characterizing the Ultrasonic Transducers

An accurate analysis of the ultrasonic transducers in U-Verse is essential to maximize the whole system efficiency. Therefore, a key issue is to understand (i) the transducer's optimal operating frequency to maximize its efficiency; (ii) the transducer's η_{e2a} conversion efficiency to derive accurate recharging times; and (iii) the transducer's impedance (decomposed in its real and imaginary parts) to design the matching circuit [43] and thus maximize the amount of power transferred to the EHU.

To investigate the above key characteristic, we needed a reliable reference scenario so as to conduct precise electro-acoustic measurements. For this reason, we have leveraged the experimental setup in Figure 5, where a signal generator produces a sine wave amplified by 24.81 dB through a Mini Circuits ZHL-6A+ connected to the transducer, which is immersed in a water tank. The ultrasounds propagate through the water and are received by a Teledyne Reson TC4038 hydrophone, used as reference and located at 1 m from the transducer. The received waveform is pre-amplified by 50 dB through a Teledyne Reson VP2000 before being measured by an oscilloscope.

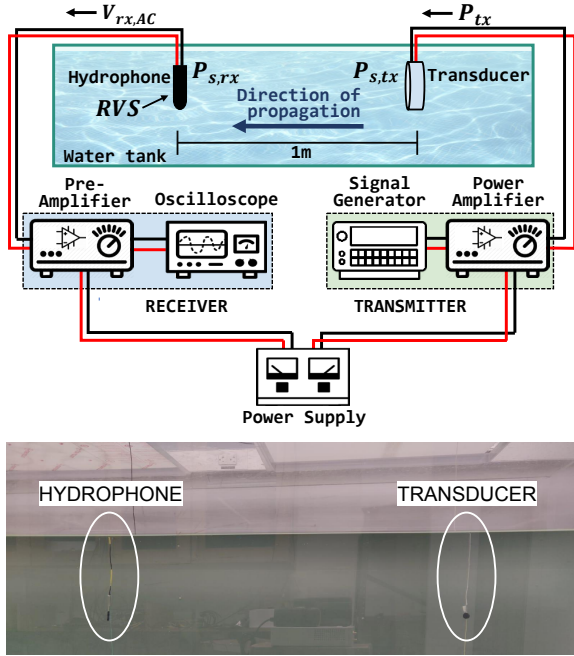


Figure 5: Experimental setup to characterize the transducer.

Ultrasonic Transducers. We utilize the custom-made ultrasonic transducers by American Piezo to generate and receive ultrasonic waves [4]. An example of these transducers was shown in Figure 2. The transducer operates around 700 kHz, and is based on a thin-disk piezoelectric element (0.95 cm in diameter and 3 mm thick) with 200 kHz bandwidth. We chose a central frequency in the order of the hundreds of kHz since it is a good trade-off between attenuation of ultrasounds in tissue (increasing with frequency), thickness of the piezoelectric element (decreasing with frequency), available bandwidth (increasing with frequency), and radiation directivity (increasing with frequency). Furthermore, a diameter of 0.95 cm is a good compromise between size, conversion loss (increasing with smaller disks), and directionality (decreasing with smaller disks).

Conversion efficiency. A transducer is characterized by electro-acoustic and acousto-electric conversion efficiency values. We now derive an expression for the transducer electro-to-acoustic (η_{e2a}) conversion efficiency. We also point out that measuring acoustic quantities would be significantly challenging, as it would require the use of high-precision instruments in water (e.g., an electronic microscope to measure the transducers displacements). Thus, we derive the acoustic quantities as functions of electrical quantities, which we can measure directly and with precision. Let us define as *sound power level* $P_{s,tx}$ the power (expressed in dB) relative to a reference value of power $P_0 = 1$ pW of a sound wave at a nominal distance of 1 m, as

$$P_{s,tx} = P_{s,rx} \cdot 10 \log_{10} \left(\frac{A_s}{A_0} \right) \quad [\text{dB}] \quad (2)$$

where $P_{s,rx}$ is the *received power level* at the hydrophone, measured in dB, A_s is a surface that wholly encompasses the transducer, and $A_0 = 1 \text{ m}^2$ is a reference area. To calculate $P_{s,tx}$ we need to

derive the received sound power level $P_{s,rx}$ that can be expressed as a function of the received voltage across the transducer $V_{rx,AC}$ and the receiving voltage sensitivity (RVS) of the transducer [42] as follows:

$$\frac{V_{rx,AC}}{M} = 10^{\frac{P_{s,rx}}{20}} [\mu\text{Pa}], \text{ where } M = 10^{RVS/20} [\text{V}/\mu\text{Pa}] \quad (3)$$

Thus, $P_{s,rx}$ is derived as

$$P_{s,rx} = 20 \log(V_{rx,AC}) - RVS \quad [\text{dB}] \quad (4)$$

Finally, by plugging Equation (4) into (2), we can derive $P_{s,tx}$ and thus the conversion efficiency as

$$\eta_{e2a} = \frac{P_{s,tx}}{P_{tx}}. \quad (5)$$

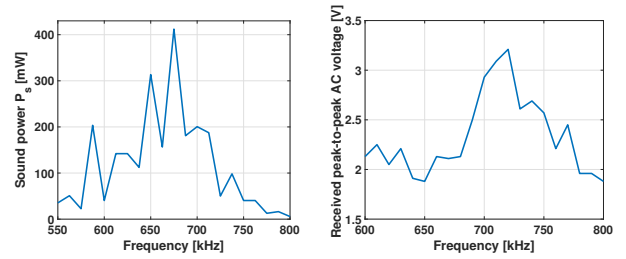


Figure 6: (left) sound power emitted by the ultrasonic transducer and (right) received AC peak-to-peak voltage, with 10 V peak-to-peak transmitted voltage, as a function of frequency.

The left and right side of Figure 6 show respectively the measured sound power $P_{s,tx}$ and the received $V_{rx,AC}$ voltage as a function of frequency. We notice that the transducer shows a peak at 675 kHz although the nominal central frequency is 700 kHz. However, we also notice that the voltage peak happens at 720 kHz. Therefore, we selected an operating frequency of 700 kHz as compromise.

3.3 Characterizing the Rectifier Circuit

As explained in Section 2, a rectifier is needed to convert the received AC signal to a DC voltage, and thus provide a DC power source to the energy storage. To this end, we use one of the simplest passive AC-to-DC power conversion circuits, the Graetz's bridge, which consists of four diodes and one smoothing capacitor.

In order to compute the efficiency of the rectifier, we measured the impedance of the transducer using a network analyzer [2] calibrated on a purely resistive 50Ω load. By assuming a resistor of value R_L is placed as load, we can then measure the efficiency of the rectifier as follows:

$$\eta_{rect} = \frac{P_{rx,DC}}{P_{rx,AC}} = \frac{V_{rx,DC}^2}{V_{rx,AC}^2}, \quad (6)$$

Figure 7 shows the rectifier efficiency as a function of different R_L values. The curves show that the conversion efficiency of the rectifier increases with smaller loads. Since in U-Verse the load is a storage component which is characterized by a relatively small resistance (tens of ohms), the rectifier can easily provide efficiency values higher than 50%.

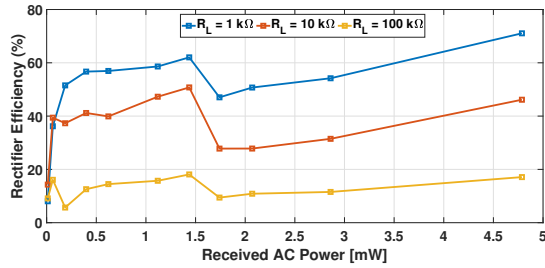


Figure 7: Rectifier efficiency for different passive loads R_L .

3.4 Matching Circuit Design

The maximum power transfer theorem, also referred to as “Jacobi’s law”, states that, to obtain maximum external power from a source with a finite internal impedance, the impedance of the load must equal the complex conjugate of the impedance of the source as viewed from its output terminals [43]. Since source and load impedances cannot be changed, a “matching circuit” must be designed to “match” them.

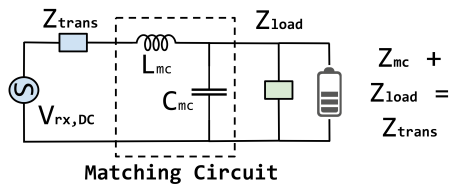


Figure 8: Schematic of the matching circuit used to maximize the amount of power transferred to the energy storage.

Figure 8 depicts a schematic of the matching circuit designed to address Jacobi’s law. Since the receiving transducer converts ultrasounds to electricity, we can model its behavior at resonance as a voltage generator with a series impedance Z_{trans} (also called Thévenin model). For the matching circuit, we decided to design a traditional L-C lumped elements matching network and intentionally used only reactive elements to avoid power dissipation in the matching circuit. To derive L_{mc} and C_{mc} , we need to accurately measure both Z_{trans} and Z_{load} (which in our case is the rectifier). Figure 9 shows the resistance (solid blue) and reactance (dashed orange) of the piezoelectric transducer (Z_{trans}) and the rectifier (Z_{load}). From the measurements in Figure 9, using a standard Smith Chart tool, we found the with $L_{mc} = 1.4$ mH and $C_{mc} = 13.5$ pF.

3.5 Relay Switch

The relay switch enables to use a single transducer for both wireless powering and ultrasonic data transfer operations, and is a unique innovative feature of U-Verse. Conversely, in systems such as [46, 47], not only does the charging have to be performed before each communication and sensing or actuation function, but the operation timings need to be carefully designed in order to distinguish between the charging and the communication phases so that they do not interfere with each other. In Figure 10 we report the schematic of the working principle of the switching mechanism. The switch is realized by means of a 1-Form-C solid state relay, specifically an

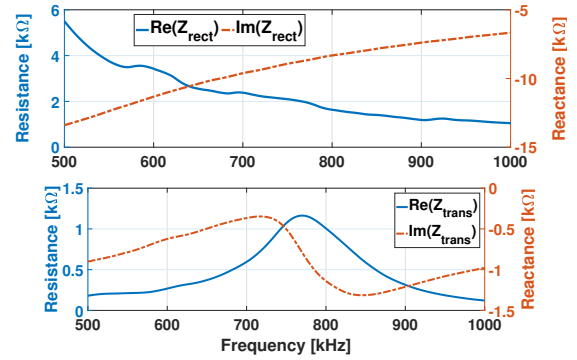


Figure 9: Measured resistance and reactance of the piezoelectric transducer (bottom) and of the rectifier (top).

LCC110 chip, which saves considerable space with respect to an electro-mechanically activated relay.

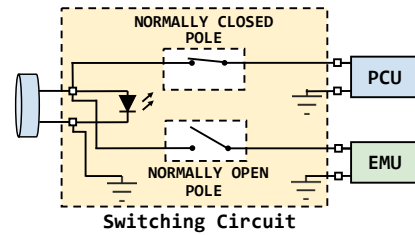


Figure 10: U-Verse charging/communication switching mechanism based on a 1-Form-C relay.

As showcased in Figure 10, a 1-Form-C relay has two internal voltage controlled switches, namely a normally closed (N.C.) pole and a normally opened (N.O.) pole. When a current is sensed by the *control line*, it activates a LED-based switching mechanism that opens the N.C. pole and closes the N.C. one. We leverage this basic principle to realize our core powering/communication hybrid technology. The transducer is connected to the control line of the relay (through the matching network), the PCU and the rectifier. Moreover, the transducer, the rectifier and the FPGA share the same ground. The PCU is “normally connected” to the transducer through the N.C. line so that it can transmit/receive with the same transducer at any time.

This is a critical design aspect because, since the transducer’s output is sensed to activate the relay, we need to make sure that, while the PCU is transmitting/receiving, the electrical signals to and from the transducer do not activate the relay. To this end, we notice that (i) the transit duration of a packet is not enough to activate the relay; and (ii) when the implant is receiving data, the received voltage is low compared to the minimum activation voltage of the relay, so it does not activate and the N.C. line remains closed allowing the PCU to receive the data. On the other hand, when the system is in recharging mode, the received voltage is high enough for the relay to activate its internal switching mechanism. Thus, the PCU gets disconnected (and, at the same time, protected from the high incoming power), and the N.O. line is closed connecting the transducer to the EHU.

3.6 Does U-Verse respect FDA limits?

It is crucial to control the transmit power to ensure that the system is compliant with the FDA exposure limitations. If the transducer had an ideal energy conversion ratio of 100% and was perfectly matched to the generator's impedance, considering the transducer surface area of $\pi(D/2)^2 = 0.71 \text{ cm}^2$, the maximum transmittable power would be 511 mW, which would lead to a superficial power density exactly equal to the FDA exposure limit. However, the transducer has a conversion efficiency of 54.3% at 700 kHz. This value was obtained from the ratio of the maximum transmitted ultrasonic power (213.4 mW) and the relative maximum transmitted electrical power (393 mW) (see Figure 11).

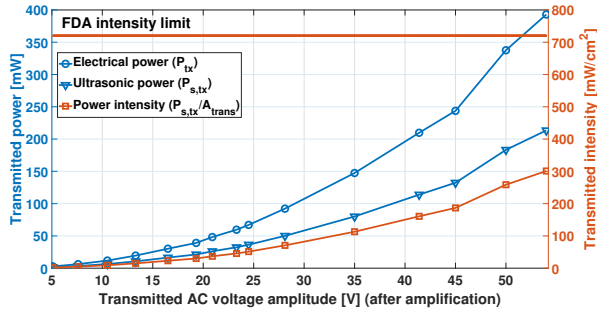


Figure 11: Transmitted power vs FDA limits.

The external charger consists of a signal generator, an amplifier to increase the transmit power, and a transducer. The active electric power delivered to the transmitting transducer coming from the amplifier is given by $P_{tx} = V_{rms} \times I_{rms} \times \cos \phi$, where V_{rms} and I_{rms} are the RMS values of the AC voltage and AC current, and ϕ the phase between the voltage and current waveforms. Figure 11 shows the transmitted power and the corresponding intensity for varying input voltage generated at 700 kHz. In particular, Figure 11 shows that even when transmitting at the highest voltage, the acoustic intensity is well below the FDA limit.

4 PROCESSING AND COMM. UNIT (PCU)

We first describe the computation and communication hardware in Section 4.1, and then discuss the ultrasonic wideband (USWB) physical-layer in Section 4.2.

4.1 Hardware

We use the 4.16 mm² Lattice Semiconductor iCE40 Ultra FPGA, which offers 4,000 look-up-tables (LUTs) and very low static current drain (71μA). For the MCU, we use a 3.2 mm² ARM Cortex-M0+ running at 48 MHz with runtime power, static power and wake-up time as low as 50μA/MHz, 2.2 μA and 7.5 μs, with 77 nA of current absorption in deep sleep. The KL03 also embeds a 12-bit ADC that can be used to interface the MCU with external analog sensors. We use a TI ADS7883 ADC operating at 2 MHz. SPI interfaces are used to connect the ADS7883 to the FPGA. SPI reduces the ADC size compared to parallel ADCs since they only use three pins for data transfer. Since the ADC operates serially on 12-bit samples with 4-bit padding, for a sampling rate of 2MHz the SPI link operates at 32 MHz, clocked by the SPI Master. To reduce energy consumption,

we use the ultra-low-power PLL included in the FPGA to internally synthesize the 32MHz clock. Since the ADC requires a 1.6V DC offset, we use a low-noise, and low power (250μA) operational amplifier (TI OPA835) to shift the signal to the desired offset. To operate at lower transmit powers we need to increase the receiver sensitivity. To this end, we use the TI AD8338, a low-noise and variable gain amplifier (VGA) offering 3 mA absorption current and a voltage controlled gain between 0–80 dB.

4.2 Ultrasonic Wide Band (USWB)

USWB PHY layer assumes time divided in slots of duration T_c , with slots organized in frames of duration $T_f = N \cdot T_c$, where N is the number of slots per frame. The transmitter includes one pulse per frame in a slot determined by a pseudo-random time-hopping sequence. Bits are mapped into a pseudo-orthogonal code of variable length, M , and code chips are mapped into pulses through pulse position modulation (PPM). Parameters (M, N) can be changed at will depending on the reliability level. Figure 12 shows an overview of the main operations of USWB. We were able to implement the circuits using 99% of the available logic cells. The receiver logic occupies more than 50% of the available resources on the FPGA, most of which is dedicated to the synchronization process.

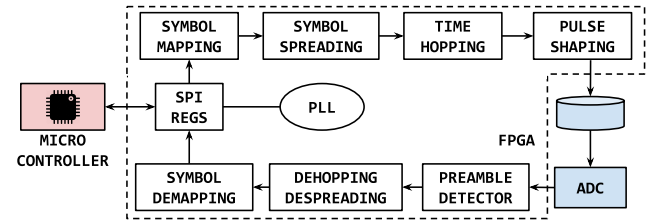


Figure 12: Overview of the main operations of USWB and its interaction with the MCU.

We now briefly summarize the main operations of USWB [38]. The data coming from the MCU is written onto SPI registers, which are then mapped into $\{-1,1\}$ binary symbols and then spread in M chips and further spread in time according to a time-hopping pattern. The incoming chips are then shaped into position-modulated pulses. The output is a train of pulses following a predefined time-hopping pattern. Finally, packets are preceded by two preambles: (i) a 64 cycles square wave that is used at the receiver for packet detection and (ii) a train of three pulses properly spaced in time used at the receiver for achieving time-hopping synchronization. After the received signal is amplified by the LNA, and analog-to-digital converted by the ADC, the packet is synchronized through a preamble. The preamble detectors consist of a packet detector for coarse synchronization and a time-hopping synchronization block for fine synchronization. After synchronization is achieved, the time-hopping deframes, the code despreads, and the demapper inverts the operation done at the transmitter.

The SPI interfaces enable communication with the external peripherals and the MCU, for both data and configurations. The data rate on this link is 1 Mbit/s, which is greater than the PHY layer data rate, such that the PHY transmitter chain is always backlogged. The ultra-low power phase-locked loop (PLL) provides a variety of

user-synthesizable clock frequencies, and is used to synthesize the 32 MHz clock signal to drive the SPI controller.

5 PROTOTYPING U-VERSE

First, we describe in Section 5.1 the design and layout of an “evaluation” printed circuit board (PCB) that was used to test the EHU module of U-Verse. Then, we describe in details a system-wide miniaturized PCB implementation of U-Verse to demonstrate that U-charge can be utilized in practical IIoMT systems.

5.1 Energy Harvesting Unit PCB Design

The EHU board shown in Figure 13 is a 2-layer PCB made of flame-retardant (FR)-4 material, which is composed of woven fiberglass cloth with a flame-resistant epoxy resin binder. We chose FR-4 since it has near-zero water absorption and is known to retain its high mechanical values and electrical insulating qualities in both dry and humid conditions. The PCB was designed using off-the-shelf components listed in Table 1. This design simplicity was chosen to assist in making the EHU a semi-open source solution available to the community. Indeed, the EHU board has a larger surface, jumpers for switching between placed modules and more breakouts that would be needed by a final miniaturized product, making this implementation currently much larger than the miniaturized U-Verse PCB described in Section 5.2.

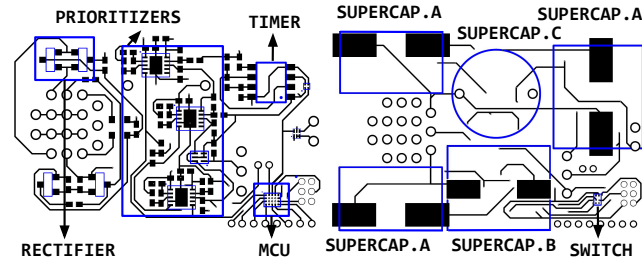


Figure 13: Energy Harvesting Unit (EHU) PCB layout; (left) top and (right) bottom side of the layout.

The platform comprises three stages. The first stage comprises (i) a Graetz’s bridge; a hybrid full-bridge rectifier integrated circuit (IC); and (iii) a Villard multiplier. The user can select which of the three modules rectifies the incoming ultrasound waves using a jumper and outputs the power to the second stage.

The second stage contains options to use a single or a cascaded reconfigurable prioritizer circuit. This circuit can be configured to only output a voltage to a connected system once a power source such as a battery or supercapacitor is charged to a certain level. These ICs on the module provide a designer using the EHU board the ability to remotely charge a main storage and one backup if the single IC is chosen and 2 backups if the cascaded IC is chosen.

The third stage contains an MCU, a timer circuit and a series of breakouts for the designer to use. The MCU and timer were provided to help researchers integrate the EHU with application-specific sensors and actuators. The MCU provides an easy SPI and I2C interface for researchers to work with as well as sleep modes and power management for peripheral devices added to the platform. The timer provides a potentially reconfigurable clock to integrate with other components such as an ADC or DAC. The timer has a

Circuit	Component	Value/Model	#
Rectifier	Diode	BAT-54A	2
	Smoothing cap.	0.01 μ F	1
Multiplier	Diode	BAT-54S	2
	Capacitor	0.01 μ F	4
Storage (1)	2-input prioritizer	LTC4419	1
	Supercapacitor A	100 mF (ESR 25 Ω)	1
	Supercapacitor B	47 mF (ESR 30 Ω)	1
Storage (2)	2-input prioritizer	LTC4419	2
	Supercapacitor C	330 mF (ESR 75 Ω)	1
	Supercapacitor A	47 mF (ESR 30 Ω)	2
Voltage reg.	LDO	TPS727	1
Control	Timer	ST TS555	1

Table 1: List of EHU PCB components.

line to the MCU so the user can also dynamically change the clock during run time for use cases such as adaptive cardiac pacing.

5.2 U-Verse PCB Design

To demonstrate that U-Verse can be miniaturized within acceptable implant physical constraints, we designed, implemented and fabricated an ultra-small (*i.e.*, 1 cm diameter) stack-up prototype PCB for U-Verse. The current prototype presents 2 PCBs, one for the PCU (top and bottom layouts respectively shown on the left and center portions of Figure 14) and one for the EHU (shown on the right side of Figure 14).

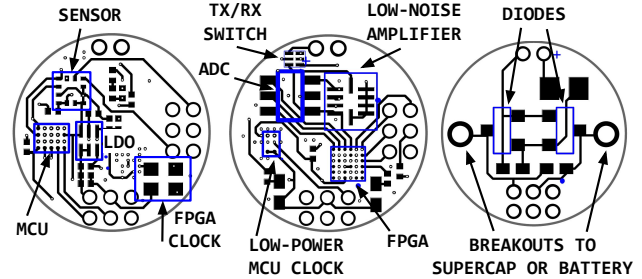


Figure 14: Miniaturized PCB Layouts; (left) top and (center) bottom side of PCU layout, (right) EHU layout.

The EHU PCB presents a Graetz’s bridge and the matching circuit described in Section 3.4, as well as a single supercapacitor and six breakouts to interface with external sensors. One of the breakouts is used to receive a pulse output from the MCU, to implement actuation functions, such as adaptive pacemaker. The PCU PCB has all the components described earlier, with in addition an ultra low-power 32 kHz clock to drive the MCU in sleep states.

5.3 PCB Design Challenges

We provide a summary of the core research challenges that were addressed when designing and fabricating the PCB.

Noise and cross-talk reduction. A key issue was to mitigate potential sources of noise and cross-talk due to the space-constrained nature of the PCB. Typically, larger devices can prevent errors caused by minor voltage differences between grounding loops as

well as the presence of leakage currents by adding a greater amount of or larger ground planes. Since the U-Verse PCB is extremely resource-constrained, the largest possible ground plane would be 1.57cm^2 which is not substantially larger than the presence of several ground loops. Thus, extra precautions were taken to isolate sensitive components, such as placing grounding guard rings around the FPGA and LNA.

Leakage paths. Naturally occurring contamination of the PCB such as deposited salts, and other debris can create leakage paths whose miniscule currents can add noise to sensitive signals such as the signal received by the ADC and FPGA. To mitigate these effects, these components are surrounded by stray conductors that offer additional paths to ground. Although our PCB has a ground plane, its small dimensions imply that each surface component as well as connector input whose ground is routed to the plane still has a significant impedance. These impedances can cause uneven grounding and harm signal integrity by introducing phase jitter. To compensate, several additional paths to ground are added to the components placed on both surfaces to the internal ground plane. This reduces the overall impedance between layers so the primary impedance seen by the system is by the internal ground plane, creating overall better grounding.

Clock lines. The constrained nature of the PCB spurred us to use a single ground for analog and digital lines – which required us physically separate analog pins and clock lines. Specifically, clock lines were placed on opposite surfaces to maximize the distance between digital lines of different frequencies. The digital lines are generated by CMOS chips which have high edge rates and which can ultimately modulate ground. For this reason, digital lines were kept exceptionally short and external clocks were placed as close as possible to the ICs – even though this posed a placement challenge with the physical board design. To prevent additional cross-talk and phase jitter internal to chips, we intentionally avoid having the MCU and FPGA sample from multiple external clocks for full power and sleep states.

6 EXPERIMENTAL RESULTS

In this Section, we evaluate the performance of U-Verse through extensive experiments. We first validate the mathematical power transfer model and study the recharging time in Section 6.1. Then, we discuss in Section the energy storage inter-charge interval in Section 6.2, finally followed by closed-loop application demonstrations in Section 6.3.

In the experiments of Sections 6.1 and 6.2, the propagation through human tissue was emulated by means of a synthetic upper arm phantom characterized by the same mechanical properties of human muscle tissues containing veins and blood. The transducers were placed on the sides of the phantom at 5 cm from each other. A water-based, acoustic adaptation gel was used to mitigate the mechanical impedance mismatch at the separation interface between the synthetic skin and the transducer coating.

Figure 15 shows the experimental testbed used to evaluate U-Verse's energy harvesting unit (EHU). The external transducer connected to the EHU via (1) transfers power or exchanges data through the phantom. The implanted transducer on the right is connected through the matching network (2) to a LCC110 relay (3). The relay

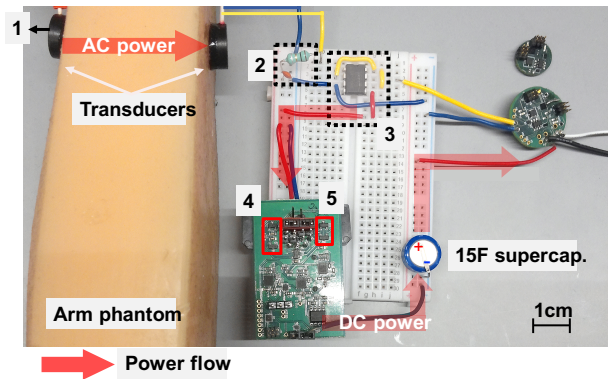


Figure 15: Experimental testbed to evaluate the EHU.

switches between the EHU (4-5) during powering and the PCU (6) during data transfer. U-Verse uses the rectifier (5) for AC to DC power conversion.

6.1 Energy Storage Charging Time

We used the experimental testbed in Figure 15 to validate our power transfer model described in Section 3.1. Figure 16 depicts the measurements and the model prediction of the energy storage charging time as function of the transmitted electrical power (mW), for capacitor storage of 15F [45] and 330mF [31]. We derived the charging times of the model dividing the energy stored in the storage component by the received power P_{rx} . The received power can be calculated as function of the transmitted power P_{tx} (which is known) using Equation (1). Figure 16 shows that not only our model is very accurate in predicting the charging times of the energy storage unit, but also that the charging time remains within acceptable limits – respectively around 10 minutes and 2 hours for the 330mF and 15F storage when transmitting at maximum power. In a real-world implantation of U-Verse, for example, the storage unit could be recharged overnight with a strap-on transducer attached to the skin of the patient. Furthermore, we would like to point out, however, that since the transmitted electrical power is still about half the amount of power allowed by the FDA (see Figure 11), the charging time of the EHU could be further decreased.

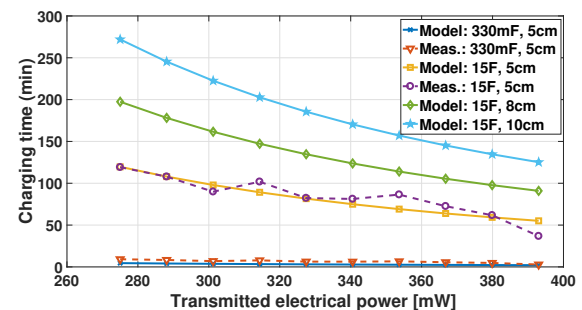


Figure 16: Energy storage charging time (minutes) as function of the transmitted electrical power (mW) for different storage sizes, measurements vs model.

6.2 Energy Storage Discharge Time

It is straightforward to notice that the energy storage discharge time strongly depends on the computation/communication/sensing burden the IIoMT application imposes on U-Verse and on the power consumption of each of these operations. This implies that it becomes necessary to define tasks and evaluate U-Verse as a function of the nature of these tasks. For this reason, we have experimentally evaluated and summarized in Table 2 the power consumption of the main operations performed by U-Verse, and also defined a set of closed-loop sensing/processing/transmission/reception tasks which are executed periodically (*i.e.*, with a duty-cycle).

Operation	Sub-Task	Power [mW]	Duration [ms]
Sensing	Sensor reading	3	1
	ADC conversion	6	.01
Processing	MCU proc.	9	1 – 5
Transmission (TX)	TX proc.	9	10
	Packet TX	10	3
	Post TX proc.	9	10
	Idle	0.006	140
Reception (RX)	Packet RX	26	600
	Post RX proc.	9	10

Table 2: Closed-loop tasks and sub-tasks in U-Verse.

Figure 17 shows an example of a closed-loop macro-task. Specifically, a macro-task composed by four operations reported in Table 2 (sensing, processing, transmission, and reception), each one of which is divided into one or more sub-tasks. A sensing operation starts with a sensor reading followed by an ADC conversion. As for the sensor we refer to an MPX2300DT1 (not included in U-Verse PCB), a biocompatible analog pressure sensor [29] that is characterized by 1 ms of response time. During this time we keep the microcontroller on, which consumes 3 mW of power (value measured experimentally). However, we do not include the powering of the sensor at this stage since it is external to the board and this powering varies from sensor to sensor. The microprocessor has an internal ADC that needs 6 mW to convert an incoming voltage signal. This task lasts 0.013 ms for the first conversion and 0.010 ms for the others. We also assume that the MCU performs some general processing that lasts 1 or 5 ms requiring 9 mW.

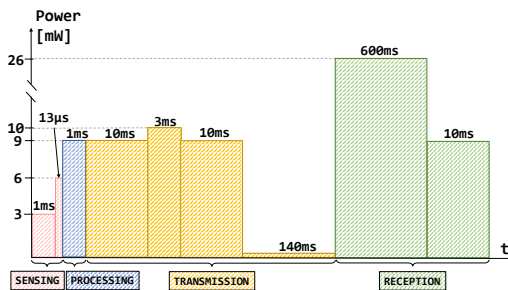


Figure 17: "Short" closed-loop macro-task.

The transmission operation starts with a 10 ms processing (different from the 1 – 5 ms mentioned above) of the data that need to

be transmitted, followed by the transmission itself. Each packet is made of a preamble followed by 16 bytes and is transmitted in 3 ms with 10 mW (we measured 6 mW to power the MCU and 4 mW for the FPGA). After the transmission other 10 ms of processing are necessary to manage the threads on the microcontroller and set the board to idle state. We choose an average idle time of 140 ms to allow the receiver to receive and process the data. After transmission, U-Verse is set in receiving mode for 600 ms, for example to receive an ACK packet. This time is justified by the fact that there is no synchronization between the transmitter and the receiver, therefore we do not know when the packet is being transmitted. The reception is the most power consuming operation and requires 26 mW (we measured 6 mW to power the MCU and the remaining 20 mW for the FPGA, ADC and low-noise amplifier). In the next 10 ms, the received packet is processed and the system is set up to start the loop again. We calculated the discharge time of the energy storage unit as a function of the duty-cycle of the macro-task, for different macro-tasks and different energy storage. We define as "short" a macro-task where we have only 1 sensor reading, 1 packet transmission and 1 packet reception, with 1ms MCU processing, while we define as "long" a macro-task with 4 sensor readings, 10 packet transmissions and 1 packet reception, with 5ms MCU processing. Transmission (TX) and reception (RX) data rates in the "short" macro-task is 20 bytes/sec in both cases, while in the "long" macro-task they are 71 and 7 bytes/sec, respectively.

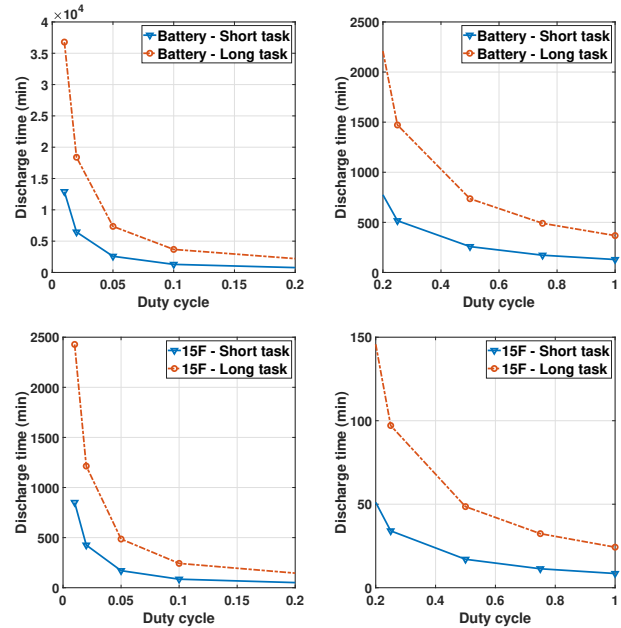


Figure 18: Discharge time as a function of the duty-cycle, for different tasks and energy storages (12 mAh battery and 15F supercapacitor).

Figure 18 shows the experimental results on the discharge time of U-Verse as a function of the duty-cycle, for both "short" and "long" macro-task, and different energy storage, *i.e.*, 12 mAh battery (PowerStream GM300910 [16]) and 15F supercapacitor. Figure 18

indicates that U-Verse is able to support discharge duration of up to 610 and 40 hours in case of battery and supercapacitor energy storage respectively when a very low duty-cycle of 0.01 is used. When both tasks are running continuously, U-Verse still support operations up to 100 and 20 minutes, respectively. In other words, with high duty-cycles, using a battery is definitely to be preferred with respect to a super capacitor. Conversely, with low-duty cycle, using a super-capacitor is to be preferred since it can be recharged indefinitely (*i.e.*, millions of times) [5].

6.3 U-Verse End-to-end Applications Demo

Finally, we report the results obtained from a demo setup that showcases an end-to-end closed-loop U-Verse application. This experiment demonstrates (i) the wireless charging of the EHU through two types of real porcine tissue, (ii) the periodic transmission of sensor data for several minutes through porcine meat; (iii) the reception of sensed data with another U-Verse PCU board; (iv) the real-time processing and plot on a computer screen; and (v) the transmission of an acknowledgment signal to U-Verse.

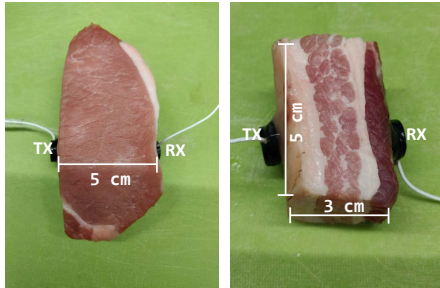


Figure 19: Experiment setups through porcine meat along 3 and 5 cm and for two different types of tissues.

To execute this demo, we used porcine meat as propagation media because it has similar properties to human muscular tissues at ultrasound frequencies. We first show wireless charging and then communication and power consumption. We tested the remote charging of the EHU along two distances, namely 3 cm and 5 cm through two different types of porcine meat, one homogeneous (on the left in Figure 19) and the other (pork belly) composed of different layers, including skin, fat and other soft tissues (on the right in Figure 19). Hereafter, we will use 30V (60V peak-to-peak) as the AC voltage amplitude applied to the charger transducer, unless differently specified. The charge times are reported in Figure 21 (left) alongside with the phantom scenario measurement and the analytical model prediction. To calculate the attenuation through the pork belly with the model in the case of 3 cm, we divided the attenuation in two parts to account for the two different types of tissues. Specifically, we chose 0.6 dB/cm @ 1 MHz for the fat part and 1 dB/cm @ 1 MHz for the other layers of tissues [3]. For the 5 cm calculation the model assumes a “soft tissue” attenuation of 0.8 dB/cm @ 1 MHz [3]. Our experimental results confirm the analytical model and show charge times between 20 and 25 minutes.

Data communication is possible at longer distances because it requires less power than wireless charging. Therefore, as showed in Figure 20, we placed a U-Verse device and wirelessly powered it to

a fully charged 15 F supercapacitor on the left side of a 12 cm long porcine meat. The transducer enclosed in a water-proof coating is connected to the U-Verse PCU through a wire, as shown in the bottom-left portion of Figure 20. Another processing and communication unit (PCU) was placed on the right side of the porcine meat and was connected to (i) another transducer similar to the one used by U-Verse, and (ii) to a PC using a modified FRDM-KL03 development platform [30], as shown on the bottom-right portion of Figure 20.

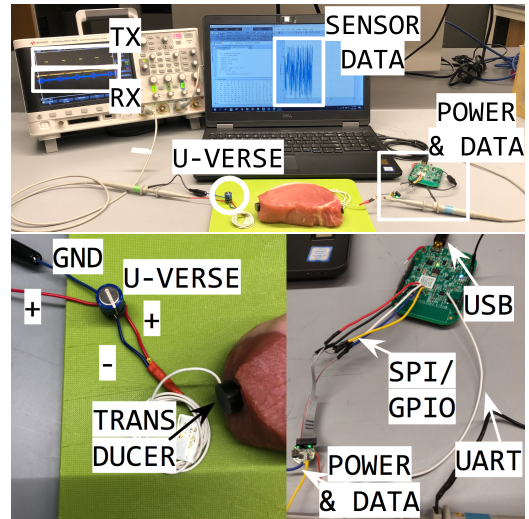


Figure 20: Closed-Loop U-Verse Application Demo.

The transducer on the right side is used both to transmit/receive data and for wireless power transfer. The FRDM-KL03 platform includes a Mini-B USB interface to connect it to a computer, SPI/GPIO and UART interfaces. We modified the FRDM-KL03 board to connect it to the U-Verse PCU. Specifically, we used the SPI/GPIO interface to transfer data from the PC to the U-Verse MCU and program it, and the UART to read data from the U-Verse PCU and send them to the computer via the USB connection. Both the MCU and the FPGA of both PCUs were programmed at the beginning of the experiment. To program the FPGAs, we used a modified version of the Lattice HW-USB-N-2B programming cable [24]. We used an off-the-shelf oscilloscope to probe the data communication interfaces of the two PCUs measuring the transmitted and received voltages (“TX” and “RX” respectively, in Figure 20). Finally, we wrote a software program to read the received sensor data from the UART interface and plot them in real time.

We implemented three different macro-tasks, where the first macro-task consisting in a “short” closed-loop operation such as the one illustrated in Figure 17. In the second and third macro-tasks, the number of packets transmitted was increased to 5 and 10, respectively. The duration of the other operations, *i.e.*, sensing, processing and reception was kept the same in the three scenarios. We measured the performances of the system in terms of discharge times that are reported in Figure 21 (right). When the system is working at maximum duty-cycle and with the shortest macro-task, it performs the worst and the supercapacitor depletes in only 7.3

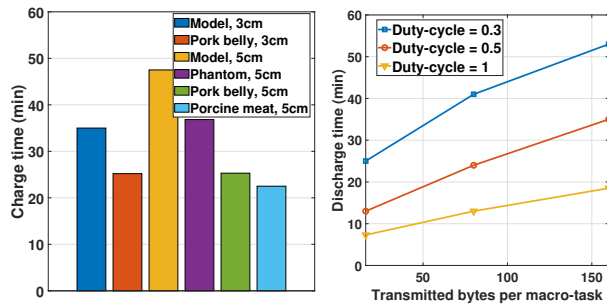


Figure 21: U-Verse charge and discharge time: (left) measured and calculated charge times for different meat types and distances; (right) discharge time as a function of the transmitted bytes per macro-task, for different duty-cycles.

minutes. Moreover, as observed in Section 6.2, the reception is the most energy consuming operation. Therefore, more frequent receptions lead to a faster discharge of the storage.

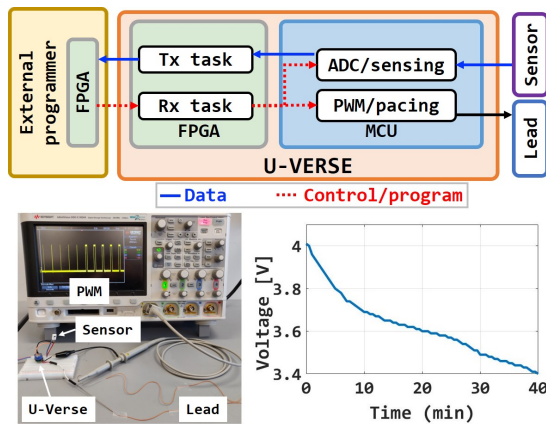


Figure 22: Reconfigurable pacemaker application demo. (Top) System logic block diagram; (bottom) experimental testbed and discharging voltage of the supercapacitor.

We finally demonstrate the versatility of U-Verse in an application-specific implementation of a reconfigurable pacemaker. Figure 22 illustrates the conceptual block diagram of the reconfigurable closed-loop pacemaker. The MCU implements three major functions: *communication* to exchange data with the internal FPGA, *sensing* to operate an ADC that receives the readings from an analogical pressure sensor, and *pulse width modulation (PWM)* to produce the pacing pulses. The pacing parameters (pacing frequency and duty-cycle) can be reprogrammed from an external device, or automatically based on the internal logic and on the values received from the sensor. The latter case is showcased in Figure 22 (bottom left). Furthermore, the sensor (*i.e.* voltage sensing threshold, acquisition frequency, and resolution) can be set and reprogrammed from an external controller. We used a 2Hz pacing rate with adjustable pulse duration, and a fixed 500 ms ADC acquisition period. To power the device we used the 15 F Vshay supercapacitor described in Section

6.1 that has an effective energy of 8 J when fully charged. The circuitry absorbs an average power of 3 mW. Figure 22 shows that the prototype can operate continuously for about 40 minutes.

7 CONCLUSIONS

Charthad *et al.* [9] recently proposed an ultrasound-powered IMD having $2 \times 3 \times 6.5$ mm dimension for wireless electrical stimulation. However, the extremely constrained nature of the passive device prohibits IIoMT scenarios where communication, computation and actuation requirements are more than what passive devices can offer. For example, a modern neurostimulator needs from 0.42 mW up to 100 mW [41], while LEDs, image sensors, and communication unit absorb up to 40 mW each in an endoscopic capsule [11]. The devices in [7–10, 46, 47] can erogate power in the order of a few milli-watts at best, and are not able to last more than few milliseconds, since their storage capability is in the order of nano-farads.

Passive RFID-based IMDs based on RF backscatter communications have also been proposed [21, 26, 44]. For example, Ma *et al.* [26] proposed an RF-based beamforming to enable powering up and communicating with RFID devices implanted in deep tissues. Vasisht *et al.* [44] proposed a backscatter design for localization of deep tissue devices. Although the above work introduces new communication strategies and technologies, ultimately they cannot implement IIoMT applications, since the generated backscatter power is usually between $1 \mu\text{W}$ and $10 \mu\text{W}$ [22], orders of magnitude less than what needed. Moreover, RFIDs backscattering leverages RF waves, which are less preferable than ultrasonic waves due to safety issues [39]. In other words, the above devices were made for “power-and-play” applications, where the IMD is powered up for a very short period of time, performs very specific, low-power tasks, and then goes to sleep. U-Verse, instead, can execute sensing/actuation applications that take longer than just few milliseconds and it can repeat them several times with a single charge. As reported in Section 6, a 12mAh battery can execute IIoMT applications with low duty cycle for 610 hours, and a 15F supercapacitor for 40 hours.

The idea of using ultrasonic waves for intra-body and underwater communications has been previously investigated [20, 32, 34, 39]. In [39], the authors proposed an Ultrasonic WideBand (USWB) physical layer protocol, and experimentally demonstrated the feasibility of ultrasonic communications in tissue mimicking material. However, the closest work to ours is [37, 38], where the authors propose two IIoMT systems based on ultrasound communications that have similar computational and communication capabilities to U-Verse. However, the platforms proposed suffer from the following core limitations: (i) they were early-stage prototypes made with off-the-shelf evaluation boards – thus, not miniaturized; (ii) the recharging problem was neglected. U-Verse is substantially different from the work proposed by Santagati *et al.* [38], because the ultrasonic communication interface is only part of U-Verse and a specific design to interface it with the EHU was necessary. We also notice that our contribution does not consist in the development of the UsWB protocol, which was done in previous work. For the first time, U-Verse addresses the above issues by presenting a rechargeable, miniaturized IIoMT platform able to support closed-loop applications. We believe that for these reasons, U-Verse provides unique contributions as it makes a substantial step toward autonomous, long-lasting IIoMT systems.

ACKNOWLEDGMENTS

We thank the anonymous reviewers and shepherd for their precious suggestions, which have helped us improve the quality of the manuscript significantly. This material is based upon work supported in part by the National Science Foundation under Grant CNS-1618731. The authors would like to thank Bernard Herrera and Flavius Pop for helping in the characterization of the piezoelectric transducers.

REFERENCES

- [1] ABHINAV SHASHANK, HIT CONSULTANT. 6 Reasons Why Healthcare Needs The Internet of Things (IoT). <http://tinyurl.com/HealthCareIoTCosts>, 2017.
- [2] AGILENT TECHNOLOGIES. Agilent ENA 2 and 4 Port RF Network Analyzers Data Sheet. https://www.brltest.com/pdf/pdf_analyzers/2160.pdf, 2006.
- [3] AMIN, V. R. Ultrasonic Attenuation Estimation for Tissue Characterization.
- [4] APC INTERNATIONAL LTD. First Steps towards Piezoaction. <https://tinyurl.com/AmericanPiezo>, 2018.
- [5] ARROW.COM. Supercapacitor vs Battery - Ultracapacitor Pros & Cons. <https://tinyurl.com/y6r4yq4l>, 2018.
- [6] BERNARD MARR, FORBES. Why The Internet of Medical Things (IoMT) Will Start To Transform Healthcare In 2018. <http://tinyurl.com/ForbesIoMT>, 2018.
- [7] CHANG, T. C., WANG, M. L., CHARTHAD, J., WEBER, M. J., AND ARBABIAN, A. A 30.5mm^3 Fully Packaged Implantable Device with Duplex Ultrasonic Data and Power Links Achieving 95kb/s with < 10⁻⁴ BER at 8.5 cm depth. In *Proc. of IEEE Intl. Solid-State Circuits Conference (ISSCC)* (2017), IEEE, pp. 460–461.
- [8] CHANG, T. C., WEBER, M. J., CHARTHAD, J., BALTSAVIAS, S., AND ARBABIAN, A. End-to-End Design of Efficient Ultrasonic Power Links for Scaling Towards Submillimeter Implantable Receivers. *IEEE Transactions on Biomedical Circuits and Systems* 12, 5 (Oct 2018), 1100–1111.
- [9] CHARTHAD, J., CHANG, T. C., LIU, Z., SAWABY, A., WEBER, M. J., BAKER, S., GORE, F., FELT, S. A., AND ARBABIAN, A. A mm-Sized Wireless Implantable Device for Electrical Stimulation of Peripheral Nerves. *IEEE Transactions on Biomedical Circuits and Systems* 12, 2 (2018), 257–270.
- [10] CHARTHAD, J., WEBER, M. J., CHANG, T. C., AND ARBABIAN, A. A mm-Sized Implantable Medical Device (IMD) with Ultrasonic Power Transfer and a Hybrid Bi-Directional Data Link. *IEEE Journal of Solid-state Circuits* 50, 8 (2015), 1741–1753.
- [11] CHEN, W., YAN, G., HE, S., KE, Q., WANG, Z., LIU, H., AND JIANG, P. Wireless Powered Capsule Endoscopy for Colon Diagnosis and Treatment. *Physiological Measurement* 34, 11 (2013), 1545.
- [12] FDA, US. Code of Federal Regulations Title 21. *Food and drugs* 5 (2010).
- [13] FOR HEALTH STATISTICS, N. C. Health, united states, 2016, with chartbook on long-term trends in health.
- [14] GALLUCCIO, L., MELODIA, T., PALAZZO, S., AND SANTAGATI, G. E. Challenges and Implications of Using Ultrasonic Communications in Intra-Body Area Networks. In *Proc. of IEEE Annual Conf. on Wireless On-demand Network Systems and Services (WONS)* (2012).
- [15] GRAND VIEW RESEARCH. Internet of Things (IoT) in Healthcare Market Size, Share Trends Analysis Report By End Use, By Component, By Connectivity Technology (Cellular, Wi-Fi, Satellite), By Application, And Segment Forecasts, 2018 - 2025. <https://tinyurl.com/y7tpepy>, 2018.
- [16] GUANGZHOU MARKYN BATTERY CO., LTD. Polymer Lithium Ion Battery Specifications. <https://www.powerstream.com/p/GMB300910.pdf>, 2007.
- [17] GUIDA, R., DEMIRORS, E., DAVE, N., RODOWICZ, J., AND MELODIA, T. An Acoustically Powered Battery-less Internet of Underwater Things Platform. In *Proc. of Fourth Underwater Communications and Networking Conference (UComms)* (2018), IEEE, pp. 1–5.
- [18] GUIDA, R., AND MELODIA, T. Ultrasonically Rechargeable Platforms for Closed-Loop Distributed Sensing and Actuation in the Human Body. In *Proc. of IEEE Intl. Workshop on Signal Processing Advances in Wireless Communications (SPAWC)* (2018), IEEE, pp. 1–5.
- [19] GUIDA, R., SANTAGATI, G. E., AND MELODIA, T. A 700 kHz Ultrasonic Link for Wireless Powering of Implantable Medical Devices. In *Proc. of IEEE Sensors* (2016), IEEE, pp. 1–3.
- [20] HERRERA, B., DEMIRORS, E., CHEN, G., GUIDA, R., POP, F., DAVE, N., CASSELLA, C., MELODIA, T., AND RINALDI, M. pMUT-Based High Data Rate Ultrasonic Wireless Communication Link for Intra-Body Networks.
- [21] IYER, V., TALLA, V., KELLOGG, B., GOLLAKOTA, S., AND SMITH, J. Inter-Technology Backscatter: Towards Internet Connectivity for Implanted Devices. In *Proc. of ACM Annual Conf. of the Special Interest Group on Data Communication (SIGCOMM)* (2016), ACM, pp. 356–369.
- [22] KONÉ, L., KASSI, R., AND ROLLAND, N. UHF RFID Tags Backscattered Power Measurement in Reverberation Chamber. *Electronics Letters* 51, 13.
- [23] KURUP, D., JOSEPH, W., VERMEEREN, G., AND MARTENS, L. In-Body Path Loss Model for Homogeneous Human Tissues. *IEEE Transactions on Electromagnetic Compatibility* 54, 3 (2012), 556–564.
- [24] LATTICE SEMICONDUCTOR. Lattice Programming Cables. <https://www.latticesemi.com/Products/DevelopmentBoardsAndKits/ProgrammingCablesforPCs>, 2018.
- [25] LUCISANO, J. Y., ROUTH, T. L., LIN, J. T., AND GOUGH, D. A. Glucose Monitoring in Individuals with Diabetes Using a Long-Term Implanted Sensor/Telemetry System and Model. *IEEE Transactions on Biomedical Engineering* 64, 9 (2017), 1982–1993.
- [26] MA, Y., LUO, Z., STEIGER, C., TRAVERSO, G., AND ADIB, F. Enabling Deep-Tissue Networking for Miniature Medical Devices. In *Proc. of ACM Annual Conf. of the Special Interest Group on Data Communication (SIGCOMM)*.
- [27] MARK WOLFF, HEALTHCARE INNOVATION. The Internet of Medical Things: Better Patient Care and Improved Clinical Management. <http://tinyurl.com/HealthCareInno>, 2018.
- [28] MELODIA, T., KULHANDJIAN, H., KUO, L.-C., AND DEMIRORS, E. Advances in Underwater Acoustic Networking. *Mobile ad Hoc Networking: Cutting Edge Directions* (2013), 804–852.
- [29] NXP SEMICONDUCTORS. MPX2300DT1, 0 to 40 kPa, Differential Compensated Pressure Sensor Datasheet. <https://tinyurl.com/y5rvseq2>, 2015.
- [30] NXP SEMICONDUCTORS. FRDM-KL03Z: Freedom Development Platform for Kinetis KL03 MCUs. <https://tinyurl.com/y373eoc6>, 2016.
- [31] PANASONIC ELECTRONIC COMPONENTS. Electric Double Layer Capacitors (Gold Capacitor) Datasheet. <https://tinyurl.com/y3klgvd2>, 2016.
- [32] POP, F. V., HERRERA, B., CASSELLA, C., CHEN, G., DEMIRORS, E., GUIDA, R., MELODIA, T., AND RINALDI, M. Novel pMUT-Based Acoustic Duplexer for Underwater and Intra-body Communication. In *Proc. of IEEE Intl. Ultrasonics Symposium (IUS)* (2018), IEEE, pp. 1–4.
- [33] POTKAY, J. A. Long Term, Implantable Blood Pressure Monitoring Systems. *Biomedical Microdevices* 10, 3 (2008), 379–392.
- [34] RESTUCCIA, F., DEMIRORS, E., AND MELODIA, T. iSonar: Software-defined Underwater Acoustic Networking for Amphibious Smartphones. In *Proc. of the Intl. Conf. on Underwater Networks & Systems* (New York, NY, USA, 2017), WUWNET'17, ACM, pp. 15:1–15:9.
- [35] RICK MARTIN, IGNITE OUTSOURCING. Internet of Medical Things (IoMT) – The Future of Healthcare. <https://tinyurl.com/yxcf336u>, 2018.
- [36] SANTAGATI, G. E., AND MELODIA, T. Sonar Inside Your Body: Prototyping Ultrasonic Intra-Body Sensor Networks. In *Proc. of IEEE Conf. on Computer Communications (INFOCOM)* (2014), IEEE, pp. 2679–2687.
- [37] SANTAGATI, G. E., AND MELODIA, T. U-Wear: Software-Defined Ultrasonic Networking for Wearable Devices. In *Proc. of ACM Intl. Conf. on Mobile Systems, Applications, and Services* (2015), ACM, pp. 241–256.
- [38] SANTAGATI, G. E., AND MELODIA, T. An Implantable Low-Power Ultrasonic Platform for the Internet of Medical Things. In *Proc. of IEEE Conf. on Computer Communications (INFOCOM)* (Atlanta, USA, May 2017).
- [39] SANTAGATI, G. E., MELODIA, T., GALLUCCIO, L., AND PALAZZO, S. Ultrasonic Networking for e-health Applications. *IEEE Wireless Communications* 20, 4 (2013), 74–81.
- [40] SAYRAFIAN-POUR, K., YANG, W.-B., HAGEDORN, J., TERRILL, J., AND YAZDANDOOST, K. Y. A Statistical Path Loss Model for Medical Implant Communication Channels. In *Proc. of IEEE Intl. Symposium on Personal, Indoor and Mobile Radio Communications* (2009), IEEE, pp. 2995–2999.
- [41] SMILEK, J., AND HADAS, Z. A Study of Kinetic Energy Harvesting for Biomedical Application in the Head Area. *Microsystem Technologies* (2015), 1–13.
- [42] TELEDYNE INC. Teledyne Marine Hydrophones Brochure. <http://tinyurl.com/TeleDyneTrans>, 2018.
- [43] THOMPSON, S. P. *Dynamo-Electric Machinery: a Manual for Students of Electrotechnics*. American Technical Book Company, 1901.
- [44] VASISHT, D., ZHANG, G., ABARI, O., LU, H.-M., FLANZ, J., AND KATABI, D. In-Body Backscatter Communication and Localization. In *Proc. of ACM Annual Conf. of the Special Interest Group on Data Communication (SIGCOMM)* (2018), ACM, pp. 132–146.
- [45] VISHAY INTERTECHNOLOGY, INC. Hybrid Energy Storage Capacitors Datasheet. <https://www.vishay.com/docs/28409/196hvc.pdf>, 2018.
- [46] WEBER, M. J., YOSHIHARA, Y., SAWABY, A., CHARTHAD, J., CHANG, T. C., AND ARBABIAN, A. A Miniaturized Single-Transducer Implantable Pressure Sensor with Time-Multiplexed Ultrasonic Data and Power Links. *IEEE Journal of Solid-State Circuits* 53, 4 (2018), 1089–1101.
- [47] WEBER, M. J., YOSHIHARA, Y., SAWABY, A., CHARTHAD, J., CHANG, T. C., GARLAND, R., AND ARBABIAN, A. A High-Precision 36mm^3 Programmable Implantable Pressure Sensor with Fully Ultrasonic Power-up and Data Link. In *Proc. of IEEE Symposium on VLSI Circuits* (2017), IEEE, pp. C104–C105.
- [48] WIRTH, J. A., AND PALEVSKY, H. I. Prostacyclin Therapy for Pulmonary Arterial Hypertension Evolves Again With the Development of an Implantable Delivery System. *Chest* 152, 6 (2017), 1100–1102.
- [49] YAN, B., DELONG, B., AN, D., KIOURTI, A., DUNGAN, K., VOLAKIS, J., MA, M., AND GUO, L. An RF-Driven Lightweight Implantable Insulin Pump. In *Proc. of IEEE Intl. Applied Computational Electromagnetics Society Symposium (ACES)* (2018), IEEE, pp. 1–2.